Mentor: Riccardo De Salvo

Mentor: Regis Dufour

Charlotte PY

Internship with LIGO Project

July 5th - December 21st 2001

Study of flex joints for the mirrors suspension

LIGO-T020065-00-D

LIGO Project
Caltech
1200 E. California Blvd,
Pasadena, CA 91125
USA

Département Génie Mécanique
et Développement
INSA
20, av Albert Einstein
69621 Villeurbanne
France

Internship context

My internship was done at the California Institute of Technology (Caltech) at the LIGO (Laser Interferometer Gravitational-Wave Observatory laboratory. LIGO is funded by the National Science Foundation, and is a joint project of physicists from Caltech and MIT with other collaborating groups at a number of other universities. It is part of an international effort towards the development of a new field of science: gravitational wave astronomy.

LIGO is a facility that should be capable of detecting for the first time gravitational waves, confirming the existence of black holes, testing Einstein's general relativity theory in the strong field limit, and opening a new window into the universe.

The LIGO project has an active experimental research effort towards developing new interferometer techniques with the extraordinary sensitivity required to detect and measure such waves.

I worked in the Seismic Attenuation System (SAS) group with Riccardo De Salvo as mentor. The SAS is charged of the mirrors suspension and seismic isolation. It is the most mechanical oriented group of the LIGO project.

My internship lasted 6 months, from July to December 2001, and gave me the opportunity to reach a good understanding of the LIGO project, and to take part in different interesting studies.

Summary

My work at LIGO consisted of mechanical and thermal analysis of mirror suspensions using finite element modeling as well as different measurements.
I first modeled and studied with ANSYS flex joints made of synthetic sapphire. I tried to optimize them with the constant concern of decreasing the dissipations.
After some more promising materials and techniques were identified, I took part in the design of a new mirrors suspension solution using glassy metal ribbons. I studied the mechanical behavior of this new kind of flex joints.
I also performed a series of thermal conductivity measurements at different temperatures on maraging steel and glassy metal samples using a crysotat device.
To finish, I took part in the design of a Quality-Factor measurement set-up which is now under construction.

Contents

1. LIGO (Laser Interferometer Gravitational waves Observatory)

1.1. What is a gravitational wave?

Gravitational waves (GW) are perturbations in the curvature of space-time that travel at the speed of light. They are created by violent events such as the collisions of stars or the vibrations of black holes. GW are emitted by accelerating masses, and propagate carrying information about their origin and about the nature of gravity.
GW have two directions of polarizations that are orthogonal to each other, and perpendicular to the direction of propagation. A free mass subjected to a gravitational wave will be stretched along one direction of polarization, and squeezed along the other one.

The existence of GW was predicted by Einstein in his general theory of relativity, and was confirmed by the observations of Joseph Taylor and Russell Hulse in the seventies. But after 30 years of active research, they have never been directly measured.

1.2. Scientific goals of LIGO

The principal goal of the LIGO Project is to detect and study gravitational waves. The data obtained will be used for research in physics and astronomy, and should lead to new discoveries about the universe. GW detection will enable to sense the matter, whether shining or dark, in the distant reaches of the cosmos. It should support studies concerning the structures of black holes, the collision of neutrons stars, and even the big bang… It will open a new window on the universe.

Pic.1: Handford observatory

LIGO research is led by Caltech, and in Massachusetts, MIT. Two observatories were built in the US: one in Hanford, Washington (which I had the opportunity to visit), and one is in Livingston, Louisiana.
Other similar projects abroad are trying to detect GW using different approaches; these include the French-Italian project VIRGO, a collaboration between Glasgow and Hanover GEO, the Japanese project TAMA, and the Australian project, ACIGA. These teams work in collaboration with each other, since observation from different locations

will enable detection of GW along all directions of polarization and will validate the measurements.

1.3. Principle of the gravitational wave detection

A gravitational wave can be detected by carefully monitoring the resulting fluctuations ΔL in the separations L between two free masses. The ratio $\Delta L/L$ is directly proportional to the wave's amplitude, which argues for large separations L (4 km in the case of LIGO). The strongest sources (i.e. black-hole collisions and supernova explosions) are likely to cause fluctuations of magnitude $\Delta L/L \sim 10^{-21}$ between free masses on earth. Considering the very small displacements to be measured, interferometry is the most efficient method.

The principle is to measure the effect of GW on mirrors acting as test-masses in the two directions of polarization of the wave. An L-shaped Michelson interferometer is used to detect the squeezing of space along one arm and its simultaneous stretching on the other arm.

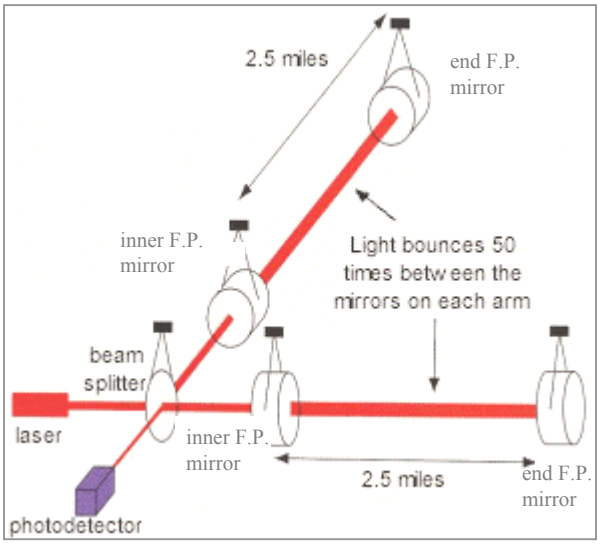

Fig. 2: Michelson interferometer used for the gravitational waves detection

Laser light enters the arms through a beam splitter located at the corner of the L, dividing the light between the two arms. The beam bounces back and force 50 times between two Fabry Perot (F.P.) mirrors before it returns to the beam splitter.

If the two arms have exactly the same length (i.e. when no gravitational wave perturbs the space-time), the interference between the two beams returning to the beam splitter will direct all the light back toward the laser. But if there is any difference between the length of the two arms, some light will travel toward a photo detector where the signal be recorded. The light propagating along the squeezed arm arrives at the vertex of the L a

little ahead of the light propagating along the stretched arm. The gravitational wave effect is detected thanks to the oscillating phase it induces shift between the two beams

1.4. Noise in GW detectors

The effects of gravitational waves are very tiny and must be distinguished from background noise sources. The major noise sources are:

- Seismic noise coming from the ground vibrations, and limiting the precision at low frequencies.
- Thermal noise resulting from thermal excitations of the mirror surface or pendular motion, at intermediate frequencies
- Shot noise such as statistic noise limiting high frequency response
- Electronic noise in the control and acquisition systems
- Problems of laser stability in frequency and intensity

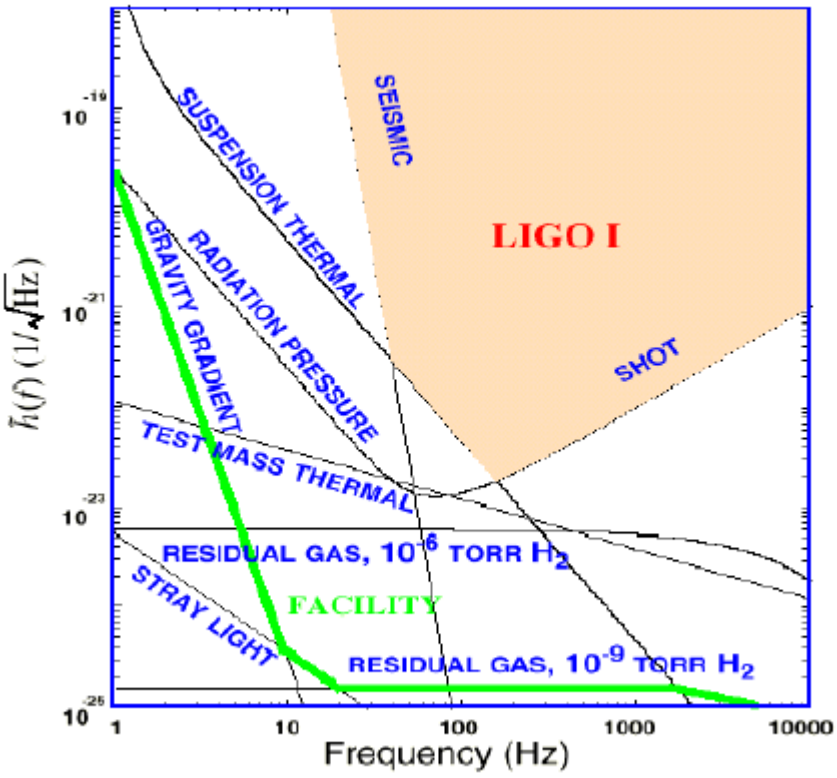

Fig.3: Graph of the different noises limiting the precision of the interferometry for LIGO I

1.4.1. Seismic noise

In order to minimize the seismic noise, which is the principal cause of test masses motion, a Seismic Attenuation System (SAS) has been designed. The SAS provides seismic isolation at low frequency, and suppresses the residual motion of the test masses for easy locking and stable operation of the detectors.

The SAS (see Fig.4) is composed of cascade of low frequency mechanical attenuators and an inertial damping control system. An inverted pendulum (IP) for horizontal isolation is fixed on a structure that is supported by tubes connected to the ground via piers. The IP hosts an ultra low frequency Geometric Anti-Spring Filter (GASF), called Filter Zero, for vertical isolation. The IP and the Filter Zero form a pre-isolator stage. Three additional GASF are attached on the Filter Zero for isolation in all degrees of freedom. An intermediate mass and the mirror are hanged under the last GASF.

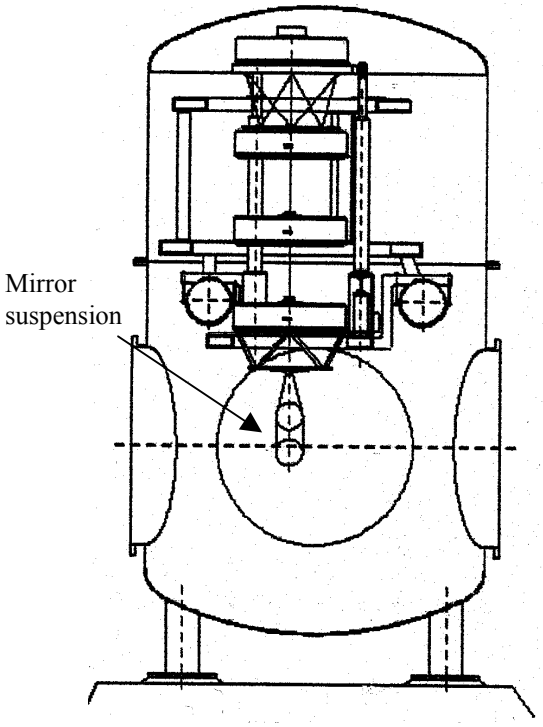

Fig.4A: complete mirror suspension inside a vacuum chamber

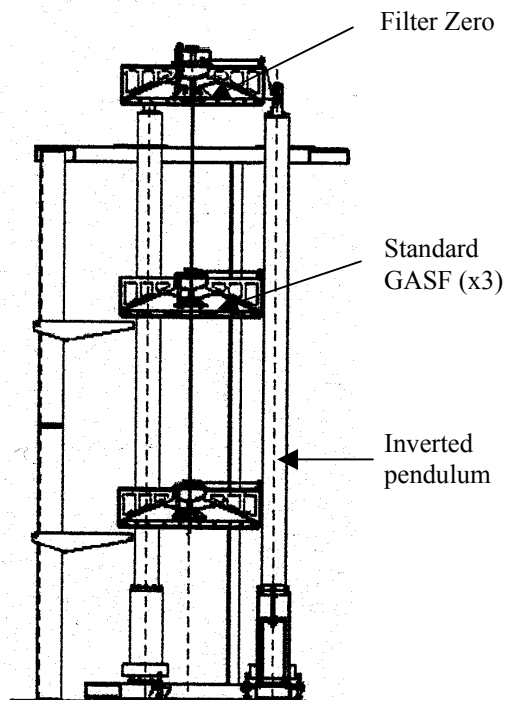

Fig.4B: zoom on the SAS chain.

1.4.2. Thermal noise

Thermal noise is one of the most serious problems of precise measurement. The thermal motions are fluctuations of generalized coordinates of the systems due to the energy stochastically flowing to and from the heat bath. One famous example of thermal fluctuations is the Brownian motion, caused by random collisions of molecules.

Thermal noise is related to dissipations. Two kinds of loss are here distinguished: external losses due to the residual gas damping (gas molecules hitting moving parts of an oscillator), and internal losses, which are the most important, coming from structural

damping and thermoelastic damping (heat flux due to temperature gradient generated by an inhomogeneous strain).

There are two kinds of thermal noise affecting interferometers. The first one is the thermal noise of suspensions. This noise generates fluctuations of the centers of mass of mirrors caused by thermal vibrations of the suspensions. The second one comes from the internal modes of the mirrors. This noise corresponds to surface deformations of the mirrors caused by thermally excited elastic vibrations of the mirrors themselves.

To minimize suspensions thermal noise, several facts are considered.
First, thermal noise is proportional to the temperature, and could therefore be reduced by working at low temperature.
Then, thermal noise is inversely proportional to the Quality Factor (Q-Factor) of the mirrors and suspensions. The Q-factor is associated to the loss at the resonant frequency and is defined as $Q = \frac{\omega_0}{\Delta\omega_0}$ where ω_0 is the resonant frequency and $\Delta\omega_0$ the half width.
The choice of materials having very high Q-Factor is a predominant concern for the design of mirrors and suspensions. That's why solutions using fused silica and sapphire have been studied for the last five years.

2. Study of Sapphire flex joints

My first work at LIGO was to design, model with ANSYS, and optimize flex joints made of synthetic sapphire. These flex joints would be used as part of the mirror suspension to minimize mechanical dissipations.
Sapphire was chosen because it has a very high intrinsic Quality Factor (10^7). Thermal noise being inversely proportional to the Q-Factor, this parameter is one of the most important in the choice of suspension materials.
Moreover, thermal conductivity of sapphire presents a peak around 30K, which could allow a good heat evacuation from the mirror in the hypothesis of a cryogenic interferometer.
(See Annex1 for sapphire properties.)

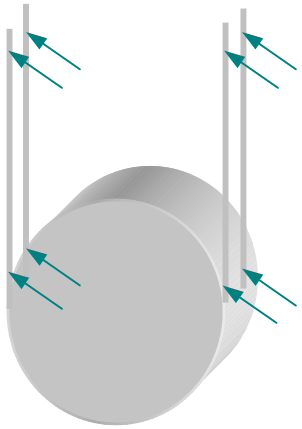

Fig.5: Flex joints locations on mirror suspensions

As explained further in this report, a more promising technique to achieve suspension with low dissipation was identified during my internship, and study of the sapphire was therefore interrupted For this reason, I will give only a brief presentation of the developments made on this subject, and will elaborate more on other aspects of my work.

2.1. What is a flex joint?

The flex joints that I consider in my studies are double flex joints; they have two thin blades perpendicular to each other, and thus allow two degrees of freedom for bending.
This enables soft movements of the mirror. The aim is to avoid energy storage inside the suspensions when the mirror is subjected to a small displacement, and thus minimize mechanical dissipations.
The flex joint, therefore, has to be as soft as possible. The objective then is to simulate with the suspension the behavior of a simple wire, using ANSYS.

Starting from an arbitrary shape, I tried to optimize the dimensions of the flex joint to reduce its stiffness, while allowing a good resistance to the traction due to the weight of the mirror. The heat dissipation from the mirror through the flex joint was also studied.

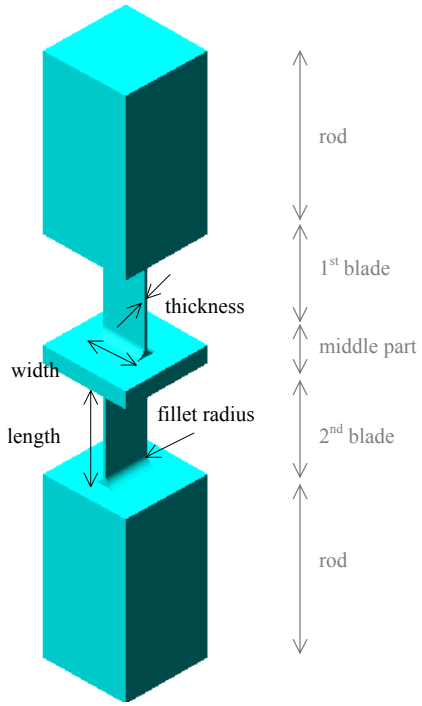

Fig.6: Definition of the parameters of a flex joint

2.2. Stiffness reduction

For all mechanical analysis on the flex joints, I built the models with ANSYS software, using finite elements SOLID95 for the meshing. My first models had a simplified geometry, with no fillet radius.

Keeping a rod section of $1cm^2$, the length, width and thickness of the blades was varied. For each model I computed the traction stress for when the flex joint is clamped at one tip and submitted to a surface load equivalent to 75N, which is a quarter of the weight of the mirror. I used a safety factor of at least 2, to check the resistance of each model.

I also calculated the stiffness of the flex joint in both directions of bending; applying an increasing transverse load at one tip of the flex joint, I calculated the transverse displacement produced where the slope of the curve "load versus displacement" is the transverse stiffness of the flex. I tried to minimize this stiffness.
I used the following criteria in order to simulate correctly the behavior of a simple pendulum, the pull-back moment due to the stiffness of the flex joint was set to at least 200 times smaller than the pull-back moment due to the gravity.

To reduce the stiffness of the flex joint, I decreased the thickness and the width of the blades. Considering those two criteria, I finally chose the following dimensions for the blades:
Length: 10 mm
Width: 5 mm
Thickness: 200 μm
(which corresponds to the shape of the flex joint shown on Figure 6.)

With this shape the maximum stress under traction is 165 MPa, the stiffness 190 N/m in one direction and 87 N/m in the other direction, and the two first natural frequencies are 22 Hz and 37 Hz.

2.3. Bending limits

For the length and width of the blade given above, I studied the bending limit of the flex joint for different blade thickness.

For each model with a given thickness, I applied an increasing transversal load until the maximum acceptable bending stress limit of 450 MPa was reached (considering the Von Mises stress). For this limit, I calculated the maximal transverse displacement and thus the maximum bending angle. Fig.7 shows the variation of bending angle with respect to the blade thickness. Increasing the thickness of the blades stiffens the flex joint, which therefore allow a smaller bending angle. These considerations can be used to implement precautionary procedures for the mounting of such flex joints.
Let's note that these maximum bending angles are given in the case of unloaded flex joints, and would reduce when traction is applied.

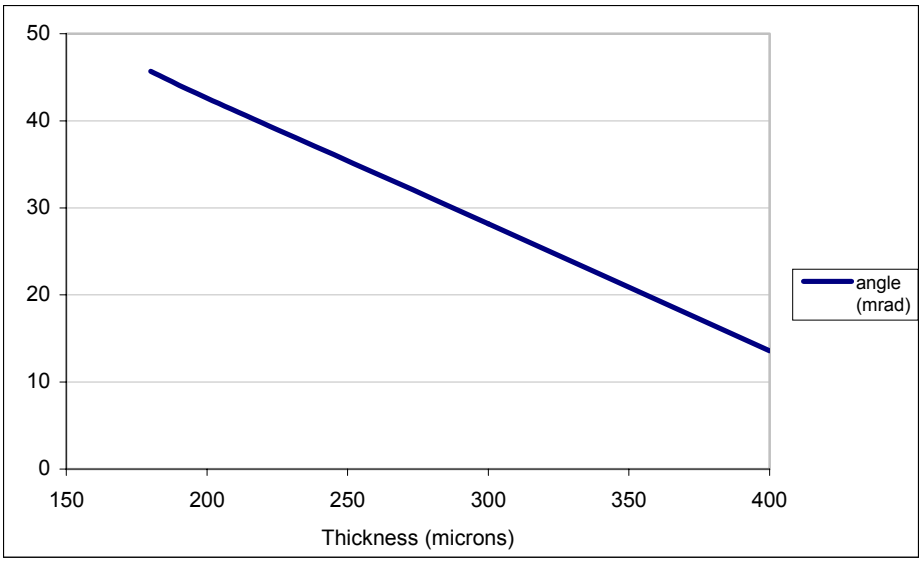

Fig.7: Maximum bending angle versus blade thickness.

2.4. Introduction of a fillet radius

In order to minimize the stress concentration at the connection corner of each blade, it is easy to machine the flex joint with a fillet radius.
It is not very convenient to draw such a model with ANSYS, so I built the geometry with AutoCAD and then exported it to ANSYS via an IGES translator.
I made the fillet radius vary keeping the total length of the blade constant, and then keeping the flat length constant. (see Fig.8). For each model, I studied the stress reduction, and also the impact on the stiffness.

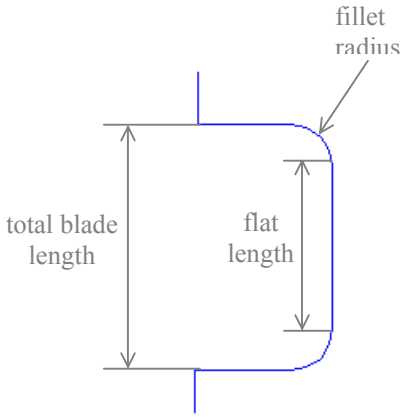

Fig.8: Definition of parameters for the variation of fillet radius.

Results are presented in Table 9.
The initial flex joint is the one presented in paragraph 2 (blade width 5 mm, thickness 200 µm). Each percentage variation is calculated with respect to this initial model.
The value of the stress is the maximum traction stress of the model: its is located at the junction corner of the blade, except for models with 5 mm fillet radius where it is located in the flat part of the blade. F1 and F2 are the two first natural frequencies.
The last row of the table corresponds to the ratio of the pull-back moments due to gravity and the stiffness effect. As explained previously, it should be at least 200.

Total blade length constant (10 mm)						
Fillet radius (mm)	No fillet	0.2	0.5	1	2	5
Flat length (mm)	10	10	9	8	6	0
Stress (MPa)	165	135	118	83	78	85
% variation		-18	-28	-49	-53	-48
F1 (Hz)	22	23	23	24	28	71
F2 (Hz)	37	38	39	41	47	121
% variation		2	4	10	24	220
Stiffness /x (N/m)	190	198	204	231	294	1942
Stiffness /y (N/m)	87	91	94	106	135	900
% variation		4	7	22	55	922
Gravity/stiffness effect	304	292	283	250	197	30

Flat length constant (10 mm)						
Fillet radius (mm)	No fillet	0.2	0.5	1	2	5
Total blade length (mm)	10	10	11	12	14	20
Stress (MPa)	165	129	102	84	80	80
% variation		-22	-38	-49	-52	-52
F1 (Hz)	22	22	21	20	18	14
F2 (Hz)	37	38	36	35	33	28
% variation		1	-6	-11	-22	-38
Stiffness /x (N/m)	190	193	178	169	158	121
Stiffness /y (N/m)	87	89	79	72	63	41
% variation		2	-6	-11	-20	-36
Gravity/stiffness effect	306	302	328	345	369	482

Table 9

Interpretation:

The fillet radius enables the reduction of maximum stress, but it also stiffens the flex joint if the total length is kept constant. Increasing the total length of the blade as well as the fillet radius presents both advantages of decreasing the stress and the stiffness, but it also means more material and thus more thermal noise.
A good compromise could be a flex joint with 10 mm total blade length, and a fillet radius of 1 mm.

2.5. Thermal analysis on flex joints

It is estimated that the impact of the laser beam on the mirror surface generates 1 Watt of heat. This flux has to be evacuated from the mirror towards the suspensions.

Moreover the idea of a cryogenic interferometer (i.e. around 4 K) might be considered, since it would enable a decrease in thermal noise, this one being proportional to $\sqrt{T}$. Under this hypothesis, the dissipation of 1 Watt of heat has a non-negligible impact and has to be carefully studied.

Since the flex joints will be the thinnest parts of the suspension, it is particularly important to study the heat dissipation inside them.

2.5.1. Equilibrium state

I conducted this study with ANSYS using the thermal analysis option. I meshed the models with SOLID90, a 3D 20 nodes element, with temperature as a degree of freedom. I performed a transient analysis with an initial condition of 4 K at all nodes of the model. Two boundary conditions were used, a heat flux of 250 mW (one quarter of the heat dissipated from the mirror) at one tip, and a constant temperature of 4 K at the other tip (this temperature stands for the cold source of the cryogenic device).

The equilibrium state is reached after about 10 minutes, and presents a maximum temperature of 8.7 K (see temperature distribution on Fig.10)

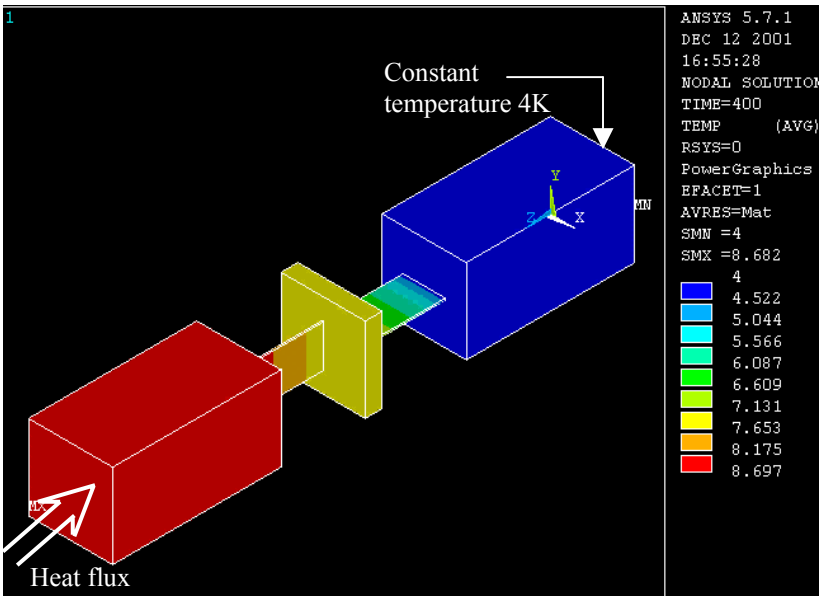

Fig.10: Temperature distribution on the flex joint.

A similar analysis performed on a complete suspension (50 cm rode with a double flex joint at each tip) leads to an equilibrium temperature of 10.9 K after more than 5 hours of transient state.

2.5.2. Sapphire conductivity

Sapphire conductivity presents a peak around 30 K (see Annex1). It is important to understand the non-linear response due to this peak.
I tried to show this effect by increasing the heat flux applied to the flex joint, and thus reaching higher temperatures.

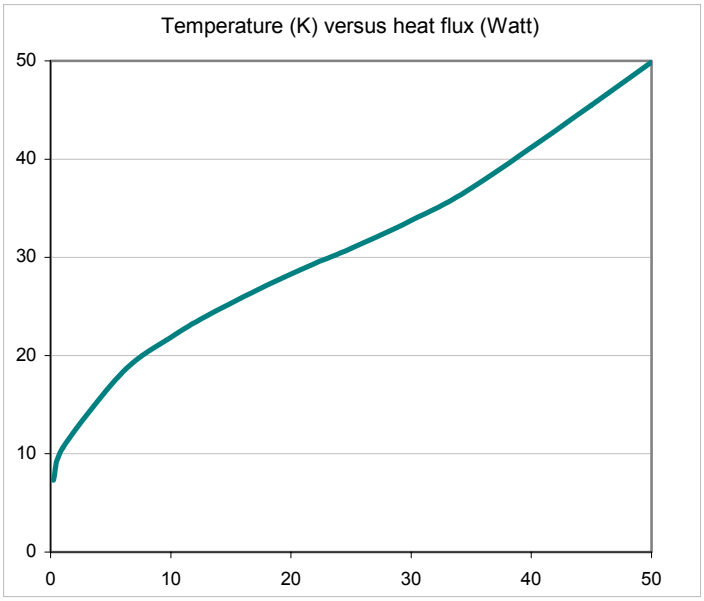

Fig.11

Fig.11 shows the maximum temperature with respect to the heat flux applied to the flex joint. It is interesting to note that the slope of the curve is higher below 17 K and above 35 K, where the sapphire conductivity is low, and the slope decreases between those two values. Between 17 and 35 K, a given increase of flux creates a smaller increase of temperature since the conductivity reaches high values.

3. Changes in the research directions

3.1. Fused silica suspensions

Several years ago, fused silica and sapphire were chosen as a material for building the mirror suspensions because they both have an intrinsic Quality-Factor orders of magnitude higher than any metal, a high Q-Factor can enable a significant decrease in thermal noise.
A recent study comparing piano wires and fused silica fibers suspensions showed that using fused silica would allow a gain factor of 3 for the thermal noise, whereas a much larger gain was expected. These results revived the interest in metallic suspensions. Several reasons limit the fused silica results: First, the suspension thermal noise comes mainly from surface stress and fused silica has a much worse surface Q-Factor than its intrinsic one. Secondly, fused silica fibers cannot be loaded more than 0.7GPa. This means building much thicker fibers, which store much more elastic energy on the surface, this energy is then available for dissipation.

All these reasons and the possibility of building very thin flex joints with metals revived our interest in metallic suspensions. We began a research on new high quality metals. The idea was that if we could find a metal with a reasonably good Q-factor, and a very high strength, we could make far thinner mirror suspensions, and therefore reduce much more the thermal noise and mechanical dissipations.

3.2. Maraging developments

Our first point of interest was maraging steel flex joints and hooks, with a geometry similar to those used earlier. The rather good Q-Factor of maraging (10^4) combined with its almost 2GPa yield point already makes it competitive. The internal Q-Factor can probably be enhanced by ion-implantation surface hardening with Carbon or Nitrogen ions. This solution is quite interesting but still requires a large amount of R&D.

3.3. Solutions using glassy metal

Our second point of interest, in which I played a more important part, was composite mirror suspensions with glassy metals for the flexures and normal metals for the structural parts.

Glassy metals are alloys that fail to crystallize during solidification, thus forming “bulk” glasses. These bulk metallic glasses have interesting properties; they are much stronger than their crystalline metal counterparts (by factors of 2 or 3), quite tough, and have very high strain limits for Hook’s elasticity law

Glassy metals are particularly easy to shape into flex joints, because they are usually manufactured in the form of spin cast ribbons that are several mm wide and 15 to 30 micron thick. It is easy to braze these ribbons to a structure and further thin the ribbon to 10 microns at the point of flexure. A mechanical study of such flex joints is presented later.

The flex joint thinning and polishing can be done by electro-polishing, which has the added advantage of selectively etching out all imperfections (possible sources of losses), micro-defects and micro-protrusions, thus decreasing the flexure noise and failure probability.

We studied several glassy metals candidates with the help of William L. Johnson from *Material Science* laboratory at Caltech.
The best option may be a Molybdenum based glass ($Mo_{38}Ru_{32}B_{20}$). It has been measured to have a yield point between 4 and 5 GPa and it is expected to allow safe loading well above 4 GPa. Although its Q-Factor was never measured several considerations point to the fact that $Mo_{38}Ru_{32}B_{20}$ should have a high Q-Factor at room temperature. The other advantage of this alloy is that it contains no iron or nickel and is not ferromagnetic. Unfortunately it is not currently commercially available. In order to get some MoRuB ribbon we are organizing a custom melt and a ribbon spin cast run with the collaboration of the *Material Science* laboratory.

4. The glassy metal option

4.1. Glassy metal membrane flex joints

Glassy metals are expected to have high Q-Factors, and are therefore promising materials for the building of new mirrors suspensions.
The glassy metal we are planning to use should be available in the form of ribbon of 30μm thickness and a few millimeters width. This is a very convenient shape to build membrane flex joints since the aspect ratio (i.e. the width of the ribbon divided by its thickness) is high. A high aspect ratio decreases the bending stiffness of the membrane, which therefore will store less energy and will generate less dissipation.

We plan to further thin the ribbon in the flex area by electro polishing from 30 to 10μm, therefore further increasing the aspect ratio.
The ribbon is left thick in both regions where it would be brazed to a structural support. The interest of having a higher thickness (which consequently increases the stiffness) is to offset the problem connected with the interface between the flex joint and the braze material which has a much lower intrinsic quality factor.

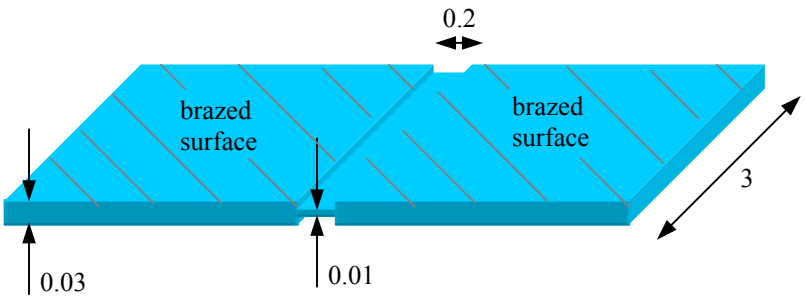

Fig.12: Shape of a glassy metal membrane flex joint. (not to scale). Dimensions in millimeters

The ribbon will be prepared already coated with an evaporated layer of brazing material on the thick areas.

These flex joints would be used in pairs, each joint along perpendicular directions. Although only a longitudinal flex joint is required to avoid the bending motion of the pendulum, a second transversal flex joint will be used to suppress the buckling effect. The pair of flex joints would be placed between a hook holding the mirror and a wire connecting the mirror to an intermediate mass. Another pair of flex joints would be placed at the other tip of the wire.

4.2. Construction of the Finite Element model

I made a finite element model of a glassy metal ribbon thinned in the middle, and brazed on one edge to a rigid structure. The ribbon is 30µm thick at both extremities and 10µm in the middle part. The length is 3mm and width 0.3mm.

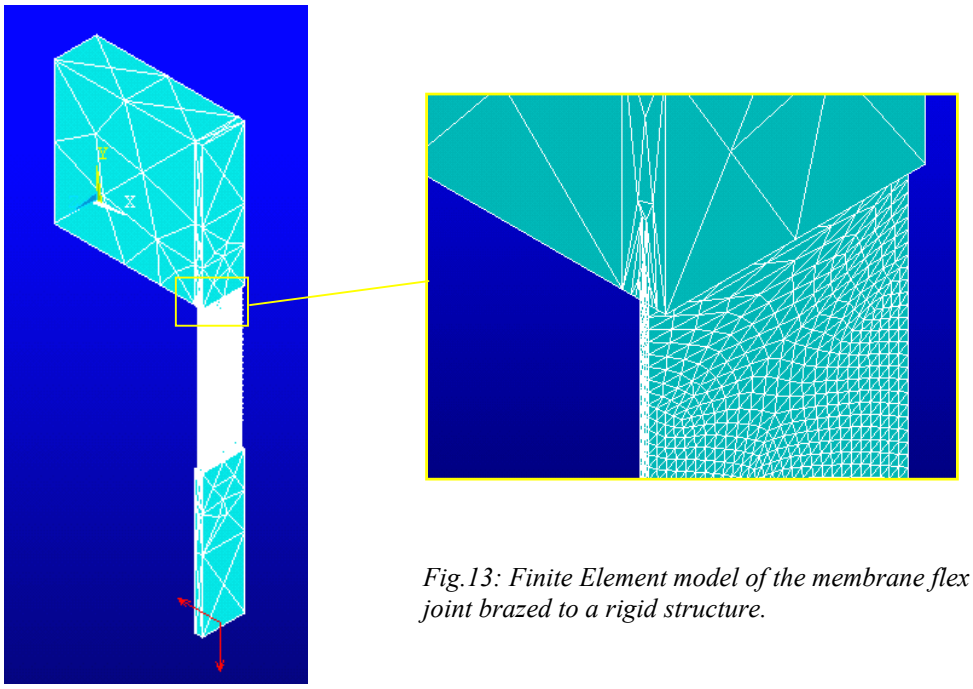

Fig.13: Finite Element model of the membrane flex joint brazed to a rigid structure.

Using the ribbon made of glassy metal, I thus used the following properties: E=350GPa, ν=0.3, and ρ=7860 Kg/m^3. The rigid structure should be of classical steel, but in order to minimize its size on my model, and thereby reduce the number of elements, I applied a fictitious higher density (10^4 Kg/m^3) and a suitable gravity load.

The brazing between the ribbon and the structure is modeled by a "glue" operation on ANSYS. A clamping boundary condition is applied on the top surface of the rigid structure.

Given the thinness of the ribbon in its flex part (30 µm) with respect to the other dimensions, the meshing was hard to do. It was necessary to have several elements even in the thickness of the ribbon in order to obtain the correct joint behavior. (see zoom on Fig.13)
This model is composed of more then 48000 "SOLID95" elements, and each round of calculations required several dozen of minutes.

4.3. Stress distribution along the surface of the membrane

I computed the stress distribution along the length of the membrane, i.e. the thinned part of the ribbon, when the flex joint is submitted to both traction and flexion. Traction representing the weight of the mirror, it is of course 1000 times higher than the flexion effect which originates from a transverse movement of the mirror.

In all the following curves, the traction stress Syy is expressed in Pa, and the abscise represents the length of the membrane, y=0 being the top and y=1 the bottom.
The internal face of the membrane is the one submitted to compression and the external is submitted to elongation.

- I first applied, at the bottom tip of the ribbon, a punctual longitudinal load (along $-\vec{y}$) of 5N, and a punctual transverse load of 10^{-3}N.

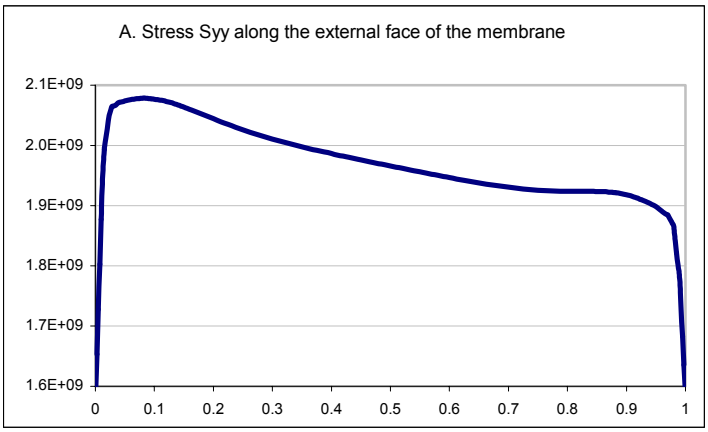

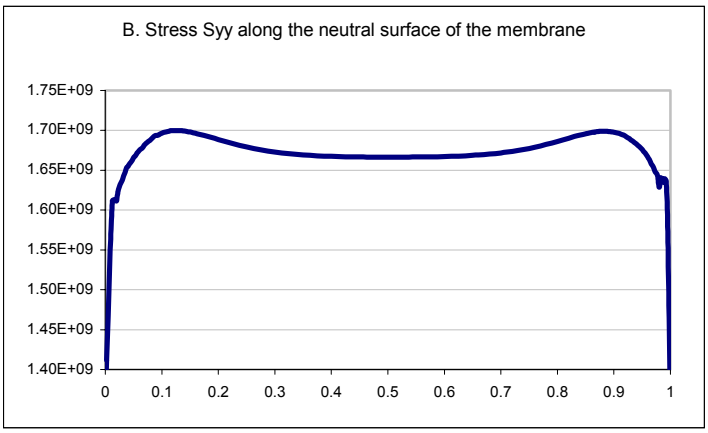

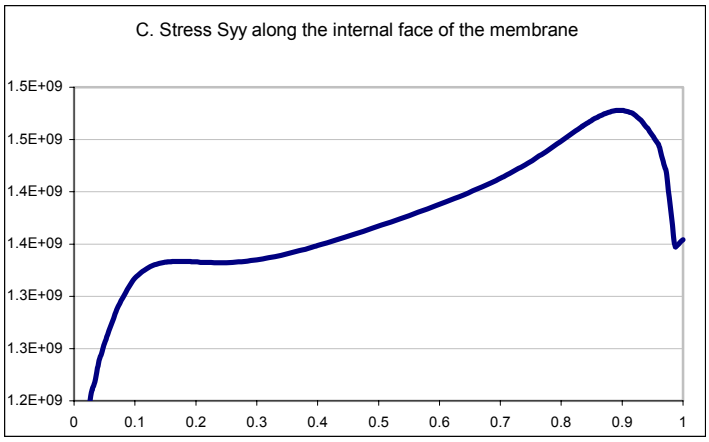

Fig.14: Stress distribution along the membrane.

In Fig.14 A and C, the slope of the curve is due to the flexion effect (traction on A, compression on C), this effect is neutralized along the neutral surface.

The stress concentration at each tip of the membrane (around y=0 and y=1) comes from the geometry discontinuity at the corner between the thick and thin parts of the ribbon. Making a fillet radius during the electro polishing can minimize this effect.

- I studied the consequence of a variation of the traction and flexion effects one with respect to the other. Fig.15.A shows that an increase of the traction (with flexion being constant) offsets the stress curve towards the top, whereas an increase of the flexion increases the slope of the curve (see Fig.15.B)

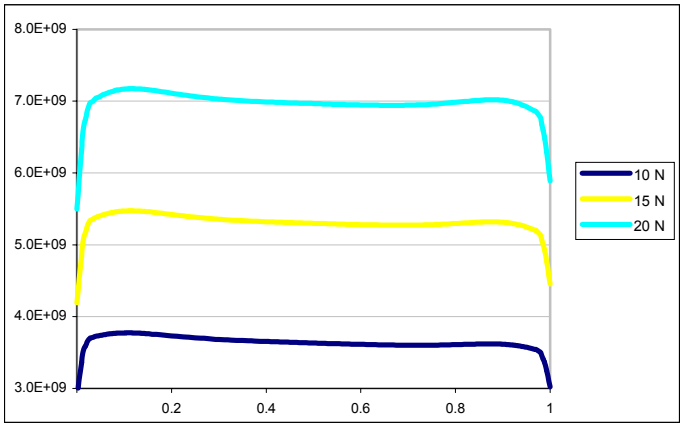

Fig.15.A: Evolution of the stress distribution when an increasing traction load is applied

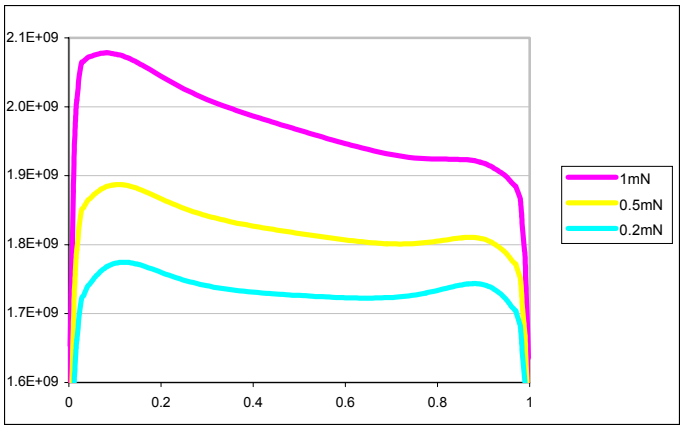

Fig15.B: Evolution of the stress distribution when an increasing transverse load is applied

4.4. Effective bending length

One interesting effect about membrane flex joints is that when it is highly loaded in traction with respect to flexion, the stress tends to be constant after a certain distance called the effective bending length. In the load case of Fig.16, all the bending effect (showed by the slope of the stress curve) is concentrated in the first half part of the flex. After this point the stress becomes constant, and the flex behaves as if it was loaded only in traction.

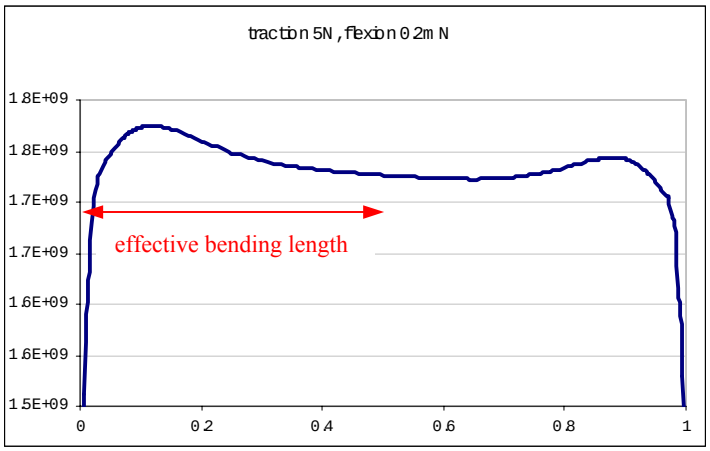

Fig.16: Effective bending length of a membrane flex joint.

For a constant flexion load (0.2mN in this study), the effective bending length decreases with the traction applied to the flex. (see Fig.17). The higher a flex membrane is loaded, the more it bends at the beginning.

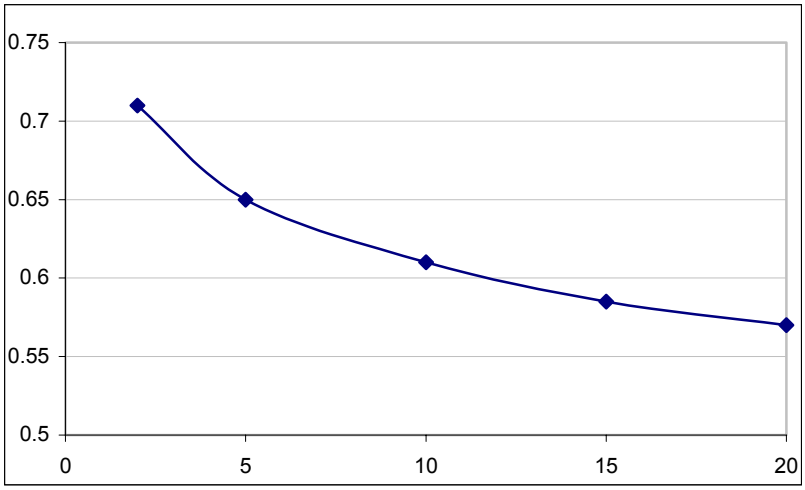

Fig.17: Effective bending length (mm) versus traction load applied (N)

4.5. Study of the brazing.

We wanted to compare the surface strain energy on the brazed interface and on the internal face of the membrane to know if the brazing will hold.

The surface strain energy is given by: $E = \frac{1}{2}\iint_S S_{yy}\varepsilon_{yy}\,dydz$

I thus calculated the stress S_{yy} and strain ε_{yy} on both surfaces. Those values being constant along z, the integration along z is reduced to a multiplication by the width of the ribbon. I performed the integration along y graphically.

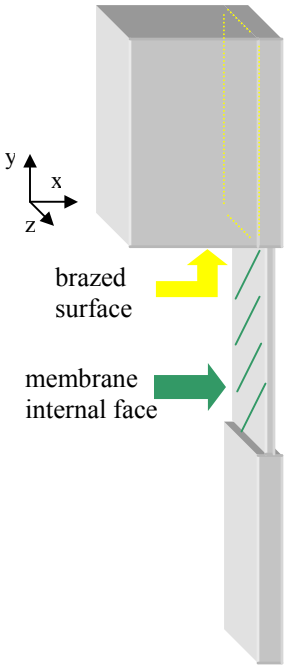

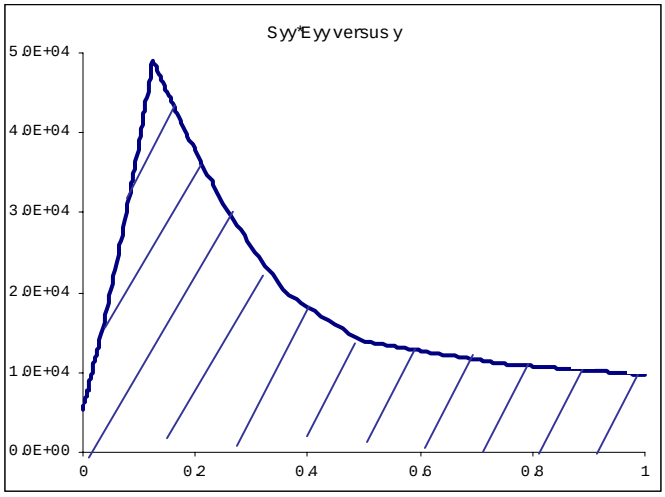

*Fig.18: Graphical integration of the product stress*strain along y on the brazed surface.*

Results:
The energy stored on the membrane internal face is about thousand times higher than on the brazed surface. This comparison leads to the deduction that the brazed surface is submitted to very small strain, and should therefore generate much less mechanical noise. Moreover, we can deduce that the brazing is efficient enough to ensure a secured and non-dissipative joint.

5. Measurements of thermal conductivity

5.1. Aim of these measurements

The aim of this research was to study the ability of several materials to conduct heat at different temperatures. Most of the materials tested (different kinds of maraging steel and glassy metals) were possible candidates for new mirror suspensions. Some other glassy metal samples were provided by our partner laboratory, the *Materials Science* of Caltech, and we were asked to study them.

Materials behavior at very low temperature (such as 4K) is not very well known, that's why these measurements were necessary and of interest for LIGO.
Moreover, measurements over a variety of temperatures allow the identification of Debye peaks and of the related loss processes.

5.2. Cryostat device

I had the opportunity to use a brand new cryostat (the Physical Property Measurement System, PPMS, from the company *Quantum Design*). The PPMS enables the measurement of thermal, electrical and magnetic properties of samples in a temperature range of 1.9K to 400K and under a magnetic field from 0 to 14 Tesla. For my measurements I did not need to use the magnetic field.

Picture 19: PPMS cryostat used for thermal conductivity measurements

The PPMS is composed of a 30L dewar containing liquid helium with a sample chamber, and a cabinet with all the control devices and pumps. The PPMS can either be controlled from the control panel on the cabinet or from a PC thanks to a specific software provided with the device.
The cryostat container has to be filled with helium. The helium transfer is a delicate operation considering the risks of gas leaks or of ice plugs. I learned the techniques of transfer and also the precautions to take with Eric Black.

The temperature of the sample can be driven as low as 1.9K with liquid helium circulation around the chamber. The sample chamber can be isolated from the thermal bath and heated to any arbitrary temperature up to 400K.
A High-Vacuum cryo-pump reduces the amount of gas in the sample chamber and thus minimizes stray thermal conduction from the heated sample.

5.3. Sample preparation

The sample can be a rod or a blade of length approximatively 20mm. It is mounted on a puck and connected with four copper leads to a heater shoe, two thermometer shoes and a cold shoe (see Fig.20). The cold shoe acts as a heat sink and also enables to fix the sample to the puck.

The copper leads are either soldered (when possible) or glued to the sample. In this case we use a two components epoxy glue that allows a very good thermal conductivity, and we cure the sample by heating it for 2 hours at 80°C.

The preparation of the samples (cutting, soldering or gluing) was a delicate job considering the precision required and the small dimensions of the leads and samples.

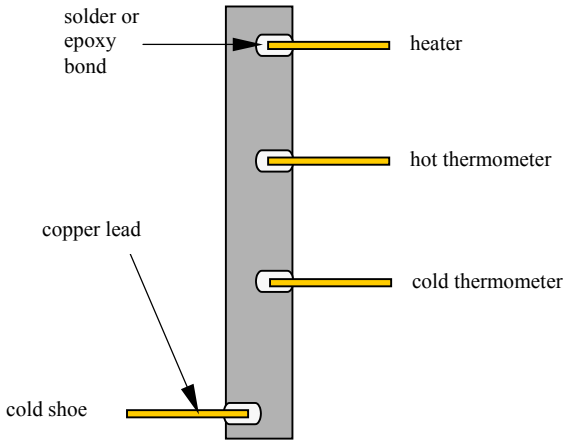

Fig.20: Sample connections

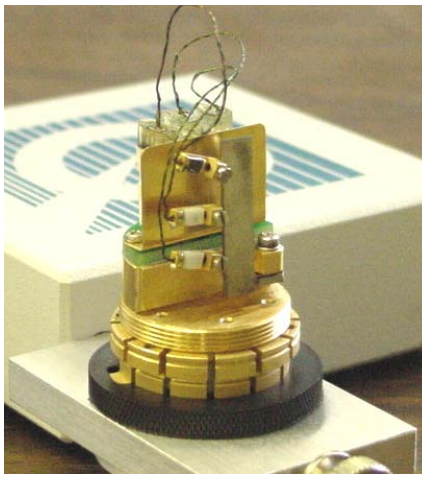

Fig.21: Sample mounted on puck

5.4. Principle of the measurement:

Heat is applied to one end of the sample by running current through the heater. The temperatures T_{hot} and T_{cold} are measured at the thermometer shoes. Heat exits the sample to the cold shoe.
The heat passes from the heater to the cold shoe through the sample, with very little losses through the two thermometer leads. This is why this technique, as opposed to a two-leads configuration, enables us to neglect the thermal resistance of the leads.

The PPMS software automatically calculates the thermal conductivity from the applied heat flux, the resulting ΔT, and the sample geometry. As the heat flux cannot de determined directly it is estimated as the power (I^2R) dissipated in the heater resistor, minus the losses due to black body radiation or thermal conduction down the leads from the shoe assemblies.

If specified, the software also measures the electrical conductivity at the same time.

5.5. How to make a measurement run

All operations on the cryostat concerning the pressure (purging and sealing the chamber, venting, creating high vacuum) or the temperature setting are controlled from the PPMS software.
For the thermal conductivity measurement I had to specify the sample material and its geometry (length between hot and cold thermometer shoes, cross sectional area between those two points, total surface of the sample and leads) as well as the approximated infrared emissivity.
Sequence files were written in order to automatically control all the operations necessary for a single measurement. The temperature was set to decrease from 300K to 10K with a certain cooling rate, and then from 10K to 1.9K with a slower rate. The temperature drop is continuously measured and the software calculates automatically the thermal (and electrical) conductivity. A graph showing the thermal conductivity versus the temperature is then generated from the data file. The whole measurement took about ten hours.

5.6. Results

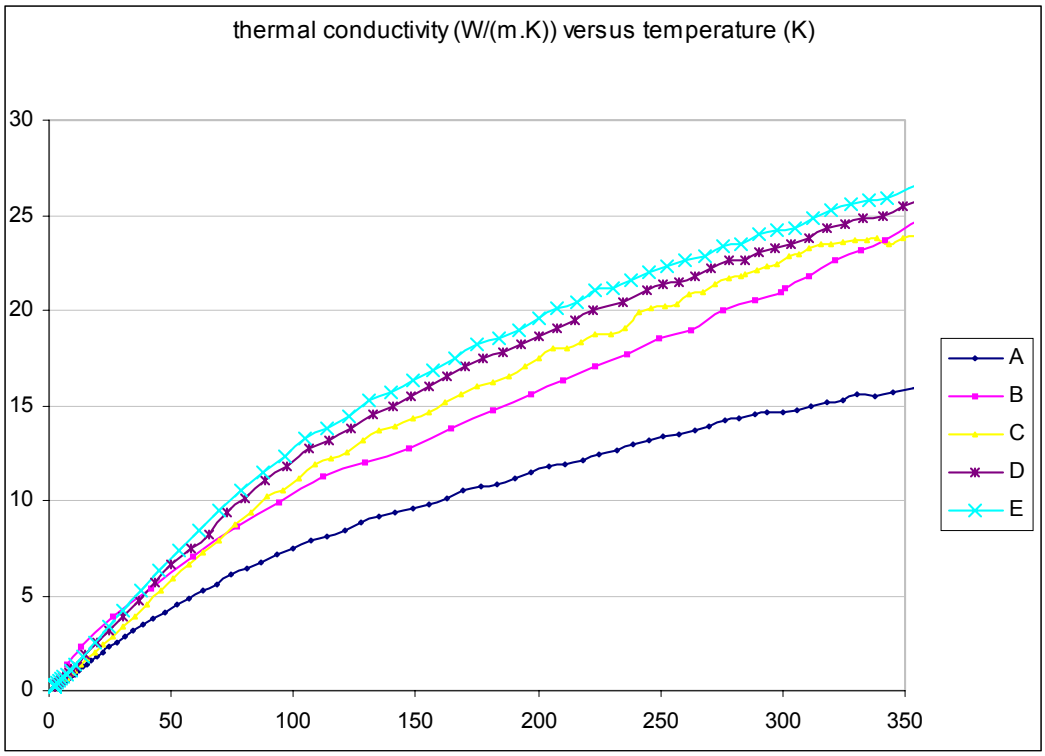

Fig.22: Comparison of thermal conductivity curves of different maraging steel samples.

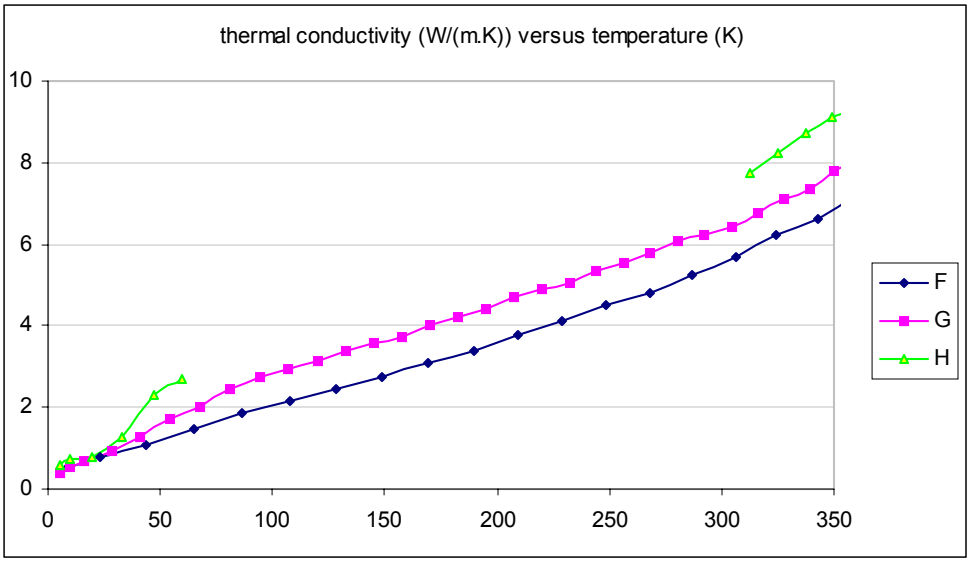

Fig.23: thermal conductivity of 3 kinds of glassy metals

Sample tested	Material	Heat treatment / Specification
A	Maraging steel "Marval 18"	solubilised at 840C
B		solubilised
C		precipitation 100h at 435C
D		precipitation 4h at 480C
E		resolubilised 1h at 850C, precipitation 16h at 480C
F	Glassy metal	Vitralloyed 1
G		Vitralloyed 1c
H		PdNiCuP

Table 24: list of samples tested

• Fig.22 shows the thermal conductivity versus temperature of several maraging steel samples that underwent different heat treatments.
These measurements show that precipitation increases thermal conductivity whereas solubilisation has the opposite effect.
The precipitation treatment extracts soluble atoms from the matrix and generates precipitation grains inside the iron matrix. The purer iron grains allow longer ballistic trajectories of the phonons through the matter. Solubilisation is the inverse process.

Thermal conductivity increases with the duration and the temperature of the precipitation.

• Fig.23 shows some results from the measurements on glassy metals.
Samples F and G are produced with a similar process, but have different percentage composition.
For sample H, despite several tests, no data points were generated by the PPMS between 60 and 310K. The probable software bug was not identified yet.

• Whatever the temperature, glassy metals have a lower conductivity than maraging steel, because the glassy structure allows only phonon diffusion and no ballistic phonon transmission.

<u>Difficulties encountered:</u>

Few results about glassy metals are presented here because many problems made their measurement difficult.

Initial difficulties encountered came from the sample preparation itself. Glassy metal are not easily weldable, I therefore had to use an epoxy glue to fix the copper leads to the sample. Despite extreme care taken while sample preparation, most bonds broke during

the mounting of the sample or presented an insufficient thermal or electrical conductivity. I had to remake dozens of samples before being able to get one good measurement.
I have not been able to measure one glassy metal ribbon called “Glassmet 2605”. This ribbon is 30µm thick only and presents an extremely smooth surface, on which nothing sticks. Even when the bonds eventually were strong enough, the measurement failed because the PPMS was unable to get a good temperature fitting.

Other problems came from the acquisition system. I very often got error codes revealing bad temperature fitting, or no data points at all. The measurement of sample H is an example of this. One possible explanation is that the glassy metal samples have typically very small dimensions and small conductivity; little heat can therefore propagate through, reaching perhaps the precision limits of the device.

I did not have sufficient time to solve all these problems or to finish the measurements.

6. Quality Factors measurement set-up

6.1. Principle of the measurement

The quality factors of different glassy metals and maraging samples will be measured at different temperatures in the new Quantum Design cryostat. For this purpose we conceived and built a system of optical measurement. The principle is to measure the oscillation of a reed excited by an electrode and mounted as shown on Fig.25.

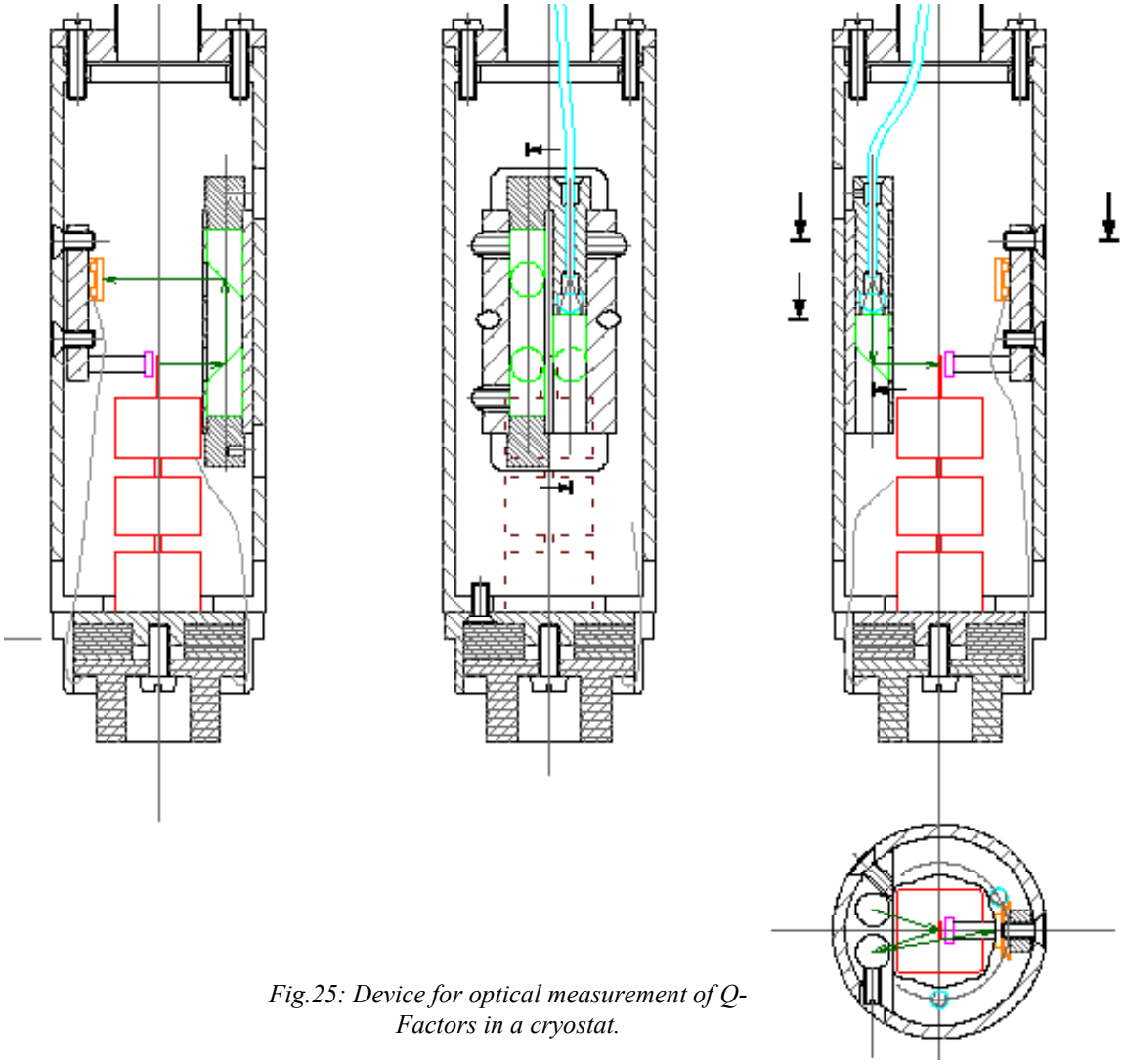

Fig.25: Device for optical measurement of Q-Factors in a cryostat.

The reed being measured is the top lip on the red structure. The red structure is monolithic, constituted by three masses, and glued on a puck. Each soft link between the masses acts as a mechanical isolator. The aim of the 3-stage chain is to avoid the damping of the reed vibrations, and therefore isolate the puck from the movements of the top of the structure. It also isolates the reed from the boil-off noise of liquid helium. This arrangement is expected to allow the measurement of high Q-factors even in the lossy environment of the cryostat.

The optical fiber (in blue) brings light to a first periscope, the light then reflects on the reed surface and is transported by the second periscope to a position sensitive photodiode (the light path is plotted in green). The reed is excited by an electrode placed on its backside. The position sensitive photodiode registers the angular displacement of the reed's tip as a function of time.

The decaying of the oscillations with respect to time enables the computation of the Q-Factor. Q is given by $Q = \omega\tau$, where τ is the decay time, and ω the pulsation of the oscillation. Since Q is proportional to the decay time, this method is appropriate for measuring high Q, which is what is expected.

The setup is designed to measure the intrinsic Q-Factors of the reed materials as a function of temperature between 2 and 350^{o}K.

For maraging steel, the test reed will be monolithic to the attenuation tower. In the case of glassy metals, which are very thin ribbons, the reed would be brazed, like in the flex joints, to a rigid ledge on the top mass.

6.2. Analysis of the mechanical isolation

6.2.1. Model construction

I built a finite element model of the 3-stage isolator in order to study the vibration attenuation. The goal was to compare the displacements of the top of the reed (point 1), to the middle mass (point 2) and to the bottom mass (point 3) when a frequency dependant load is applied on the top of the reed (this load represents the electrode excitation).

I first modeled the isolation tower according to the design, which meant introduction of the clamping boundary condition to be set on the bottom of the lowest mass (model A on Fig.26). Then I realized that in order to know the displacement of the lowest mass, this boundary condition was not appropriate. The lowest mass should be free. But a harmonic analysis with ANSYS requires boundary conditions.
Therefore I built an adapted model (model B on Fig.26) in which the lowest mass is free but linked to a flexible blade clamped to the ground.

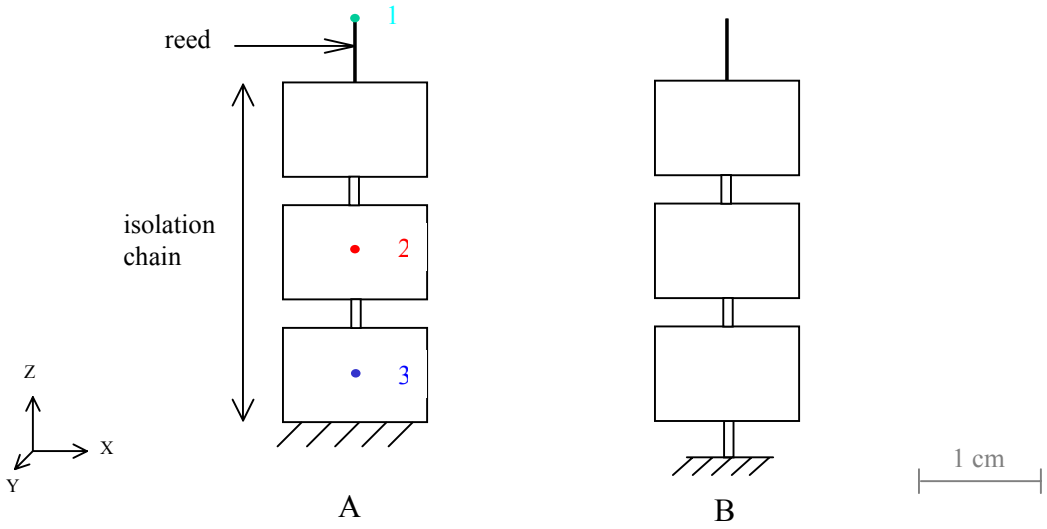

Fig.26: A/ Real model of the isolation chain. B/ Adapted model for the transfer function calculation

6.2.2. Analysis

I performed a modal analysis followed by a harmonic analysis. The modal analysis provided with the natural frequencies and the associated mode shapes of the model.

	Frequency (Hz)	Mode Shape
F_1	**66**	Rotation around **y**, at lowest blade
F_2	129	Rotation around **x**, at lowest blade
F_3	250	Twist around **z**, at lowest blade
F_4	**388**	2 nodes oscillation around **y**
F_5	694	2 nodes twist around **z**
F_6	751	2 nodes oscillation around **x**
F_7	**896**	3 nodes oscillation round **y**
F_8	1001	3 nodes twist around **z**
F_9	1730	3 nodes oscillation around **x**
F_{10}	**3222**	Rotation around **y** of the reed

Table 27: first natural frequencies of model B

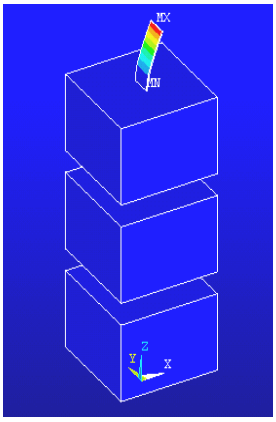

Fig.28: deformed shape at F_{10}=3222Hz

The frequency F_{10} corresponds to the oscillation of the reed around the y-axis, and is therefore the main frequency of interest. The modes F_1, F_4 and F_7 also present

displacements along x, and therefore could have intervened in the harmonic analysis. Even if they could present displacements along x, I did not consider mode shapes with frequencies higher than F_{10}, because these modes will be isolated even better than F_{10}.

I performed a harmonic analysis, with the mode superposition option using 10 modes. I calculated the displacement Ux1, Ux2 and Ux3 at points 1, 2 and 3 respectively, for a frequency range of 100 to 4000 Hz. See Annex 2 for the analysis procedure.

Figure 29 shows the displacements Ux1, Ux2 and Ux3 versus the frequency. The resonance peaks corresponding to F_4 and F_7 and F_{10} are clearly visible.
At 3222Hz, we reach an attenuation factor of 10^3 between the top of the reed (point1) and the middle mass (point 2), and a factor of 10^4 between the top of the reed and the lowest mass (point3): if the top of the reed oscillates with an amplitude of 100µm, we can expect a displacement of less than 10nm at the bottom of the isolation tower, which should not disturb the measurement.

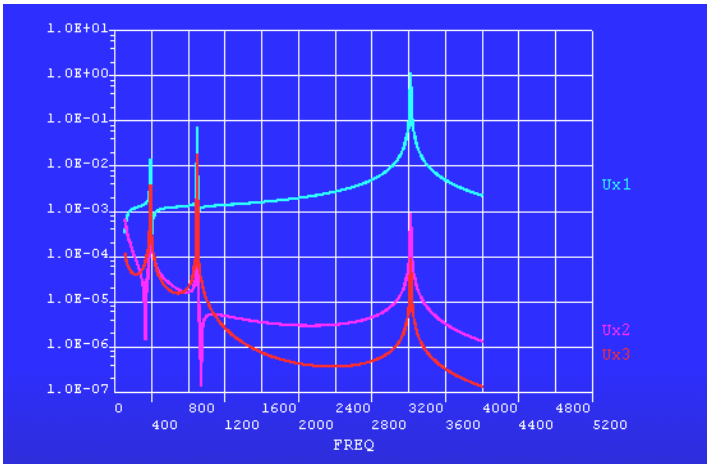

Fig.29: Displacements at points 1, 2 and 3 versus frequency

Fig.30 represents the ratio of these displacements versus frequency, which is the transfer function. The parameter Hij is defined as Ui/Uj.
This graph enables us to read directly the attenuation factor between the top and the bottom. It is interesting to note that the F_{10} resonance peak is not visible on the ratio plot, since the 3 points have the same behavior around this frequency.

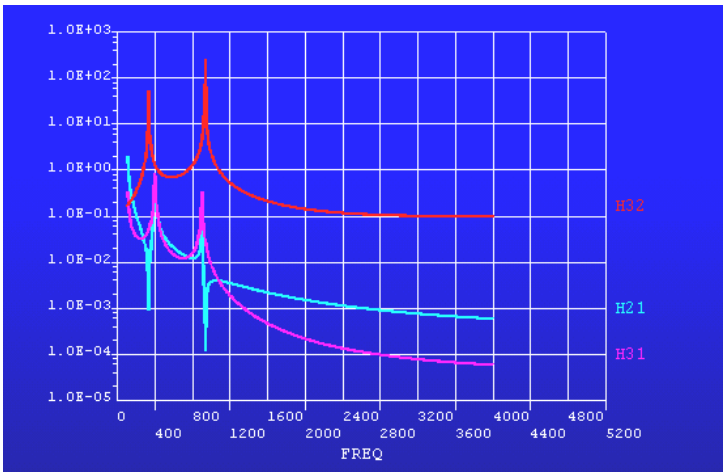

Fig.30: Transfer Function versus frequency. (Hij=Ui/Uj)

This analysis enabled us to show that the isolation tower we had conceived was efficient to attenuate the vibrations of the reed, and allows a good hold-up of the sample on the puck.
We are now going to build a prototype of this model, and we will test it. If the attenuation reveals to be insufficient, it is possible to improve it by making bigger masses and thinner connecting blades.

6.3. Conception of the measurement device

My contribution to this project also consisted of taking part in the design and testing of the device. We conceived the setup but the final drawings were made in Italy. I ordered the different pieces like laser, position sensitive diodes, lenses, optical fibers and adapters for the cryostat flange. I also tested these components.
At the end of my internship the building and assembly of this device is still not finished, I will therefore not be able to run the measurements myself.

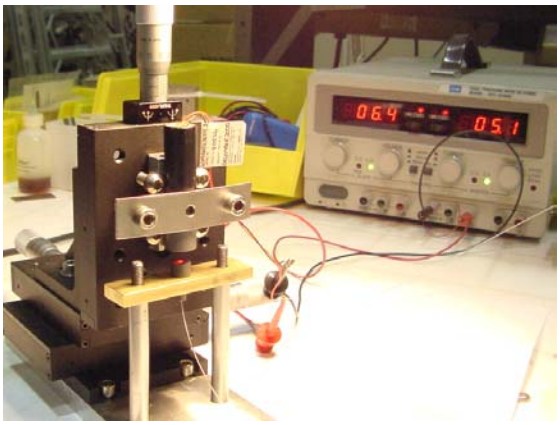

Picture 31: Testing of the laser and optical fiber.

Conclusion

My work during this internship enabled to test two possible scenarios for the mirrors suspension.
My analysis on sapphire flex joints gives a good knowledge of its performances, and could be used further if sapphire becomes the material of choice again.
The solution using glassy metal ribbons seems promising and still requires research and development efforts.
The thermal conductivity measurements will be pursued on other glassy metal samples.
Some technical problems with the cryostat still have to be fixed.
The Quality Factor measurement set-up is now under construction and should provide very interesting information about the efficiency of different materials for the mirrors suspension.

Acknowledgments

I would like to thank my mentor Riccardo De Salvo who gave me this great opportunity to work at LIGO and to learn a lot in various subjects.
Thanks also to Virginio Sannibale for his many explanations and his kindness.
Thanks to Helena Armandula for her help with the sample preparation and to Eric Black for his advice on the crysotat.
I would like to thank all the members of the LIGO team for their welcoming attitude.
To conclude, thanks to Regis Dufour and Alain Berlioz for their help with ANSYS.
This research is supported by the National Science Foundation under Cooperative Agreement PHY98-011583.

Bibliography

Stresses in flexure pendulum for gravitational wave detectors
L. Ju, D.G, Blair
Physics Letters A, May 1999

Q factor measurements on prototype fused quartz pendulum suspensions for use in gravitational wave detectors
S. Rowan, S.M. Twyford, R. Hutchins, J, Kovalik, J.E. Logan, A.C. McLaren, N.A. Robertson, J. Hough
Physics Letter A, September 1997

Pendulum Mode Thermal Noise in Advanced Interferometers: A comparison of Fused Silica Fibers and Ribbons in the presence of Surface Loss
A.M. Gretarsson, G.M. Harry, S.D Penn, P.R Saulson, W.J. Startin, S. Rowan, G Cagnoli, J. Hough
Physics Letters A, April 2000

Elastic and anelastic properties of Marval 18 steel
F. Cordero, F. Corvasce, R. Franco, G. Paparo, E. Maiorana, P. Rapagnani, F. Ricci, S. Braccini, C. Casciano, R. De Salvo, F. Frasconi, R. Passaquieti, M. De Sanctis, A. Solina, R. Valentini
Journal of Alloys and Compounds. Ref:310 (2000) 400-404.

Material test for the suspension subsystem
F. Gutong, S. Braccini, C. Casciano, V. Dattilo, R. De Salvo, F. Frasconi, G. Gennaro, R. Passaquieti, R. Valentini
CNRS, INFN, & VIRGO internal report. Ref: VIR-TRE-PIS-4600-129. June 1997

The creep problem in the VIRGO suspensions: a possible solution using Maraging steel.
M. Beccaria, M. Bernardini, S. Braccini, C. Bradaschia, G. Cagnoli, C. Casciano, G. Cella, E. Cuoco, V. Dattilo, G. De Carolis, R. De Salvo, A. Di Virgilio, G.T. Feng, I. Ferrante, F, Fidecaro, F. Frasconi, A. Gaddi, L.Gammaitoni, A. Gennai, A. Giazzoto, L. Holloway, J. Kovalik, P. La Penna, G. Losurdo, S. Malik, S. Mancini, F. Marchesoni, J. Nicolas, F. Palla, H.B. Pan, F. Paoletti, A. Pasqualetti, D. Passuello, R. Poggiani, P. Popolizio, M. Puntoro, F. Raffaelli, V. Rubino, R. Valentini, A. Vicere, F, Waharte, Z. Zhang
Nuclear Instruments & Methods in Physics Research, Section A. June 1997

The Q-factor of flexure membranes
M. Baker, L. Ju, D.G, Blair
Institute of Physics Publishing, August 2001

Ultrahigh Q pendulum suspensions for gravitational wave detectors
L. Ju, D.G, Blair, M. Notcutt
Review of Scientific Instruments, July 1993

High Sensitivity accelerometers for gravity experiments
A. Bertolini
Ph.D Thesis, July 2001

Study of the Thermal noise caused by inhomogeneously distributed loss.
K. Yamamoto
Ph.D. Thesis, December 2000.

Annex 1: Sapphire mechanical and thermal properties

Density:	3970 Kg/m^3
Poisson's ratio	0.29
Young's Modulus	350 GPa
Shear Modulus	175 GPa
Compressive strength	2 GPa
Flexural strength	900 Mpa
Tensile strength	350 Mpa
Specific heat	750 J/(Kg.K)

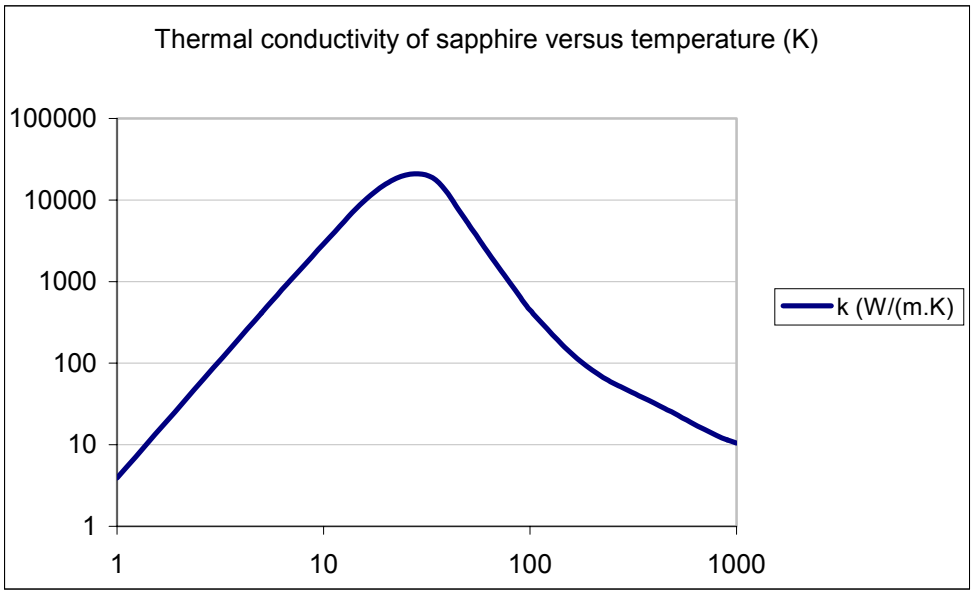

Annex 2: Program for the harmonic analysis

(used in section 6.2.2)

```
/SOLU
ANTYPE,MODAL
MODOPT,SUBSP,11,0,0, ,OFF
RIGID,
SUBOPT,5,4,6,100,5,ALL
/STATUS,SOLU
SOLVE
FINISH
/SOLU
ANTYPE,HARMIC         ! HARMONIC ANALYSIS
HROPT,MSUP,10         ! MODE SUPERPOSITION USING TEN MODES
HARFRQ,100,4000,      ! RANGE OF FREQUENCIES FROM 100 TO 4000 HZ
F,504,FX,1,
KBC,1                 ! STEP BOUNDARY CONDITIONS
NSUBST,500
OUTPR,,NONE
OUTRES,,1
SOLVE
FINISH
/POST26
FILE,,rfrq
LINES,2000
PRCPLX,1
NSOL,2,504,U,X,Ux1
NSOL,3,3817,U,X,Ux2
NSOL,4,4209,U,X,Ux3
STORE,MERGE, ,
QUOT,5,3,2, ,H21, , ,1,1,
QUOT,6,4,2, ,H31, , ,1,1,
QUOT,7,4,3, ,H32, , ,1,1,
/GROPT,LOGY,1
/GRID,1
/GTHK,CURVE,1
PLVAR,2,3,4
```